This is a previous version of the article published in International Journal of Hydrogen Energy. 2015, 40(37): 12674-12686. doi:10.1016/j.ijhydene.2015.07.135

Electroactivity of Pt_x–Sn_y/C catalysts synthetized by formic acid reduction as a function of Sn content (alloy and non-alloy) for alcohol oxidation in fuel cells

F.E. López-Suárez[a,]*, C.T Carvalho-Filho[a], A. Bueno-López[b], J. Arboleda[c], A. Echavarría[c], K.I.B. Eguiluz[a], G.R. Salazar-Banda[a]

[a] *Electrochemistry and Nanotechnology Laboratory, Research and Technology Institute/Processes Engineering Post-graduation, Universidade Tiradentes, Av. Murilo Dantas, 300, Aracaju, SE, Brazil*

[b] *MCMA group, Department of Inorganic Chemistry, Faculty of Sciences, University of Alicante, Ap. 99 E-03080, Alicante, Spain*

[c] *Grupo Catalizadores y Adsorbentes, Instituto de Química, Universidad de Antioquia U de A Calle 70 No. 52-21, Medellín, Colombia*

Emails:

F.E. López-Suárez: franzedwin@gmail.com

C.T Carvalho-filho: trivellatoc@hotmail.com

A. Bueno-López: agus@ua.es

J Arboleda: jocare@gmail.com

A. Echavarría: adriana.echavarria@udea.edu.co

K.I.B. Eguiluz: katlinbarrios@gmail.com

G.R Salazar-Banda: gianrsb@gmail.com

[*] Corresponding author:

Email: franzedwin@gmail.com

Tel.: +55 079-3218-2115

Fax: +55 079-32182190

ABSTRACT

A series of Pt_x–Sn_y/C catalysts with different atomic ratios (x:y = 1:1, 2:1, 3:1) and diameters (~4 nm) were easily synthesized by a deposition process using formic acid as the reducing agent. Catalyst structure and chemical composition were investigated by scanning electron microscopy (SEM), transmission electron microscopy (TEM), X-ray powder diffraction (XRD), and X-ray photoelectron spectroscopy (XPS). XRD and SEM showed that the geometric environment was changed with Sn addition to the *fcc* Pt crystallites by forming a solid solution of Pt–Sn alloy phase for Pt_1–Sn_1/C catalyst, while for Pt_3–Sn_1/C and Pt_2–Sn_1/C, a decrease in Pt 4f binding energy was observed, and from the XPS results was attributed to charge transfer from Sn to Pt. From TEM results, it could be seen that Pt nanoparticles could be easily synthesized, even at a high metal load, without the use of expensive surfactants. The electrochemical behavior of catalysts during ethanol oxidation in acidic media was characterized and monitored in a half-cell test at room temperature by cyclic voltammetry, chronoamperometry, and anode potentiostatic polarization. The amount of Sn added affected the physical-chemical characteristics of the bimetallic catalysts; however, these catalysts did not show differences in the electrocatalytic activity towards ethanol oxidation. The presence or absence of alloy was a function of the Sn content on catalysts for the preparation method used. The behavior presented for Pt_x–Sn_y/C catalysts can be attributed to the so-called bifunctional mechanism, and to the electronic interaction between Pt and Sn.

Keywords: Platinum; Tin; Alloy; Ethanol Oxidation Reaction; Fuel Cell.

1. Introduction

Interest in the development of fuel cells as power sources in portable electronic devices and electric vehicles has been increasing in recent years. The proton-exchange membrane fuel cells (PEMFCs) are the most promising because they are clean, silent, and efficient power sources [1]. In this kind of cell, hydrogen displays the best performance as a fuel; however, the problems in the storage, handling, and distribution are important barriers to its direct use. Hence, the direct use of liquid fuels in the cell has been investigated as a possible alternative to hydrogen [2].

Among the various liquid fuels that can be used in PEMFCs, ethanol is the most promising because it is a renewable and safe molecule, and it is easy to store and handle [3]. The main disadvantage of ethanol comes from its molecular structure since it has two carbons with different functionalities, one containing a primary alcohol function and another with a methyl group. Its molecular configuration induces a hard conversion of ethanol into carbon dioxide due to the difficulty in both cleaving the C–C bond and the complete oxidation of the methyl group using platinum as an electrocatalyst [4].

In order to enhance the catalytic activity of this catalyst towards alcohol oxidation, a secondary metal is usually introduced as a co-catalyst. A Pt–Sn catalyst is generally considered the best anode for ethanol oxidation. While Pt-based anodes are the best catalysts for alcohol oxidation in acid medium, Sn provides surface oxygen species for the oxidation of CO or carbonyl species adsorbed on adjacent Pt, which are produced during the dissociative adsorption of ethanol on Pt active sites at low potentials [5–9]. Moreover, the addition of Sn contributes to reducing the amount of noble metal in the anode of direct alcohol fuel cells, which remains one of the challenges of making the technology possible. The use of tin as a co-catalyst led to interesting results compared to other bimetallic catalysts.

Pt–Sn catalysts with optimized compositions and structures have been reported to exhibit an enhanced activity [10–13]. Nevertheless, the origin of the promotion effect due to the presence of Sn in the Pt–Sn catalyst towards ethanol oxidation is still under debate and some contradictions are found in the literature [5, 11, 13–23]. Generally, it can be established that the Pt–Sn/C electrocatalysts performance depends strongly on the preparation procedures, Pt:Sn atomic ratio, and the amount of alloy of Sn in the catalyst composition.

Pt–Sn catalysts supported on carbon are commonly prepared in the absence of thermal treatment, and, as a consequence, a crystalline face-centered cubic Pt–Sn alloy and/or Sn oxides can be formed. The relative amounts of Pt–Sn alloy and SnO_2 affects the electrochemical activity of these catalysts. The effects of either alloyed Sn with Pt or adding SnO_2 to improve catalytic activity have been controversial. Delime et al. [10] prepared bimetallic non-alloyed Pt–Sn catalysts and observed that the presence of non-alloyed Sn led to increased current densities during the ethanol electro-oxidation. Jang et al. [13] compared the catalytic activity of a partially alloyed Pt–Sn catalyst with that of a quasi-non-alloyed Pt–SnO_x catalyst, and the Pt–SnO_x catalyst showed higher catalytic activity during ethanol electro-oxidation than the Pt–Sn alloy. The improvement in the activity suggests that the unchanged lattice parameter of Pt in the Pt–SnO_x catalyst is favorable for ethanol adsorption, and the tin oxide present in the vicinity of Pt nanoparticles could provide active oxygen species to remove the CO-like ethanolic residues and clean the Pt active sites. Colmati et al. [15, 16] and Zignani et al. [17] prepared the carbon-supported Pt–Sn alloys by the formic acid method, and found that the activity of these catalysts for the ethanol oxidation reaction seems to depend on the amount of both non-alloyed and alloyed Sn, in addition to the overall content of Sn in the catalyst. Others reports [5, 14, 18-20, 24] show that a good degree of alloying between Pt and Sn leads to the highest electrocatalytic activity towards ethanol electro-oxidation.

Both the preparation procedures and the Pt:Sn atomic ratios influence the performance of Pt–

Sn/C electrocatalysts. Lamy et al. [5, 25] suggested an optimum composition for Sn in the 10–20 mol.% range for catalysts prepared by a co-impregnation-reduction method, varying from 90:10 to 50:50 (Pt:Sn). Zhou et al. [9] reported the optimum composition as being 33–40 mol.% of Sn, depending on the direct alcohol fuel cell operation temperature. Jiang et al. [22] showed that Pt–Sn/C electrocatalysts with Pt:Sn molar ratios of 66:33, 60:40, and 50:50 were more active than electrocatalysts with 75:25 and 80:20 molar ratios. Spinacé et al. [26] investigated the activity of Pt–Sn/C electrocatalysts with varied Sn contents during ethanol oxidation, and showed that the electro-oxidation of ethanol begins at low potentials (~0.25 V) for 50:50 and 25:75 Pt:Sn molar ratios, with similar current values in the range 0.25–0.40 V. Above 0.4 V, the electrocatalysts with a Pt:Sn molar ratio of 50:50 displayed a superior performance. Wang et al. [27] studied the activity of Pt_x–Sn_y/C catalysts with different atomic ratios (x:y = 1:1, 2:1, 3:2) towards ethanol oxidation, establishing that the addition of Sn strongly improves the activity depending on the Sn content and the operating temperature. At lower temperatures, Sn-rich catalysts exhibited better performance, while at higher temperatures, Sn-poor catalysts gave a better performance. Finally, continuous efforts towards the development of different synthetic methods based on colloids [28, 29], co-deposition [14], microemulsions [30], sonochemistry and microwave irradiation [31–33], polyol method [22], Bönneman method [34], Pechini–Adams [35], and a sol–gel method for the purpose of improving the catalytic activity of electrode materials have been realized.

In this work, a series of Pt_xSn_y catalysts supported on carbon that could be used as anode catalysts for oxidizing ethanol in a direct ethanol fuel cell (DEFC) were synthesized by a co-deposition reduction method using formic acid as reducing agent. As the physical-chemical properties and electrocatalytic activity of these catalysts during ethanol oxidation depend on the preparation method, the Pt:Sn atomic ratio, and the amount of alloy and/or non-alloy of Sn, this study investigated the effect of amount of tin in the production of alloy and non-alloy of Sn and their relationship with electrocatalytic activity of Pt–Sn/C catalysts. The catalysts were characterized by scanning electron microscopy (SEM), transmission electron microscopy (TEM), X-ray powder diffraction (XRD), and X-ray photoelectron spectroscopy (XPS), while the electrocatalytic behavior of these catalysts during ethanol oxidation in acid medium was studied by cyclic voltammetry, chronoamperometry, and quasi-stationary potentiostatic polarization.

2. Experimental

2.1 Preparation of catalysts

The carbon support used was carbon black Vulcan XC-72 (*Carbot*) with a BET area of 240 $m^2 g^{-1}$. The catalysts consisted of 20% (w/w) metal ($Pt_x + Sn_y$) on carbon with a nominal Pt:Sn molar ratio of x:y = 1:1, 2:1, 3:1, and Pt/C was used as a reference. The catalysts were prepared by a deposition process using formic acid as the reducing agent [15, 17, 36].

The carbon support was added to 2 M formic acid solution and heated to 85°C. $SnCl_2 \cdot 3H_2O$ and/or $H_2PtCl_6 \cdot 6H_2O$ solutions were slowly added to the carbon suspension, and the slurry was maintained at 85°C for 6 hours. The suspension was left to cool to room temperature, and the powder was recovered by filtration, washed with ultrapure water until no chloride ions could be detected, and dried at 60ºC. All chemicals were analytically pure and used as received (Sigma Aldrich, purity > 98%).

2.2 Characterization of catalysts

The crystalline structure was determined by X-ray diffraction in an XPert PANalytical Empyrean Series II with Solid State Detector Pixcel-3D using CuKα radiation (0.1541874 nm). The diffractograms were registered at 2θ angles from 10º to 90º, with a scan step size of 0.01313º and a time per step of 50 s. The working conditions of the powder diffractometer were tension of 45 kV and current of 40 mA.

XPS characterization was carried out in a VG-Microtech Multilab 3000 electron spectrometer using a Mg-Kα (1253.6 eV) radiation source. To obtain the XPS spectra, the pressure of the analysis chamber was maintained at $5 \cdot 10^{-10}$ mbar and the binding energy (BE) scale was adjusted by setting the C1s transition to 284.6 eV.

Transmission electron microscopy images were obtained using a JEOL (JEM-2010) microscope at 200 kV. A few droplets of an ultrasonically dispersed suspension of each catalyst in ethanol were deposited on a copper grid with lacey carbon film, and then dried at ambient conditions for TEM characterization. Particle size distributions were based upon ~200 particles for each catalyst. The mean particle diameter, d, was calculated as:

$$d = \frac{\sum(k) n_k d_k}{n}$$

where n_k is the frequency of occurrence of particles with size d_k.

The microstructure and atomic ratios of the Pt_x–Sn_y/C catalysts were analyzed in a JEOL JSM-6490 LV Scanning Electron Microscope with high sensitivity semiconductor back-scattered electron detector and energy dispersive X-ray analyzer (EDS) detector for analysis of micro areas.

2.3 Electrochemical measurements

Electrochemical measurements were performed at room temperature using an Autolab Model PGSTAT 302N potentiostat/galvanostat. Experiments were carried out in a glass cell (one compartment) using a conventional three-electrode configuration (half-cell), and boron-doped diamond (BDD) electrodes, prepared by the Centre Suisse d'Electronique et de Microtechnique

SA (CSEM), Neuchâtel, were used as substrates for the electrocatalytic materials [37]. The boron content was ~800 ppm, and the area of the working electrode exposed to the solution was 0.08 cm^2. The reference system consisted of a hydrogen electrode in the same solution (HESS) connected by a Luggin capillary, and a Pt coil (0.5 cm^2) was used as the counter-electrode. All potentials were referred to the reversible hydrogen electrode (RHE). Nitrogen gas was bubbled through all solutions for 15 min before starting each electrochemical test.

The catalyst ink was prepared by mixing 8 mg catalyst powder, 1 ml water (Milli-Q system), and 200 µl Nafion® solution (5 wt.% Aldrich solution), which was dispersed in an ultrasonic bath. The catalyst suspension (40 µl, 3.4 $\mu g_{metal}/cm^2$) was transferred with an injector to a BDD electrode and the electrode heated to 60 ºC for 10 min.

Electrochemical activity tests were performed in aqueous 0.5 M H_2SO_4 solutions containing 0.5 M C_2H_5OH at room temperature. Cyclic voltammetry experiments were performed between 0.0 and 0.8 V (*vs* RHE) until stationary responses were obtained, then two voltammetric cycles were performed between 0.0 and 1.3 V (*vs* RHE) at a scan rate of 0.02 V s^{-1} to evaluate the behavior of each electrocatalyst. Chronoamperometric experiments were performed at 0.6 V (*vs* RHE) and anode polarization curves obtained between 0.2 and 0.8 V (*vs* RHE) in the potentiostatic mode, with all data points obtained after 200 s of polarization at each potential.

2.3 CO stripping

The CO voltammetric stripping experiments were performed as follows. CO was adsorbed onto the electrode surface by bubbling high-purity CO through 0.5 M H_2SO_4 solution, while holding the electrode potential at 0.05 V (*vs.* RHE). After the adsorption period (5 min), the dissolved CO was removed from the solution by bubbling high-purity nitrogen through the solution for 30 min while still holding the potential at 0.05 V (*vs.* RHE). The potential was then scanned in a positive direction from 0.05 V to 1.0 V (*vs*. RHE) at 0.01 V s^{-1}.

3. Results and Discussion

3.1 Physical-chemical characterization of electrocatalysts

3.1.1 XRD characterization

Figure 1 shows the X-ray diffraction pattern (XRD) for Pt_x–Sn_y carbon-supported catalysts prepared with formic acid in different nominal Pt:Sn atomic ratios and the Pt/C catalyst used as reference. All of the XRD patterns show the typical characteristic peaks of a crystalline face-centered cubic (fcc). The typical *fcc*-Pt diffraction peaks in all catalysts appear to be broadened due to an effect of small particle size. The Pt phase from (111), (200), (220), and (311) planes appear at the corresponding diffraction angles in good agreement with the Pt standard (JCPDS PDF 04-0802 reference included in Figure 1). The diffraction peak observed at 2θ = 21–27º in all XRD patterns is attributed to the (002) plane of the hexagonal structure of Vulcan XC-72 carbon. The corresponding diffraction peaks at 33º and 51º are assigned to SnO_2 (1 0 1), and (2 1 1) planes, respectively, indicating that Sn has been introduced into the Pt_x–Sn_y/C catalysts as SnO_2, as well as demonstrating that Sn nanoparticles were initially formed and then subsequently converted to SnO_2.

The average size of the catalyst particles was calculated from the Gaussian-fitted Pt (220) peak according to Scherrer's equation. The average particle size and lattice parameter are given in Table 1, which shows that ~3.0–4.0 nm Pt–Sn particles were produced. The Pt (220) diffraction peak was used as the reference so as to avoid possible disturbances from the carbon black [38]. In the case of Pt_1Sn_1/C catalyst with the highest Sn content, the typical (220) peak of the fcc-Pt structure was too broad, which might be attributed to a great diminishment of Pt crystalline properties by a too-large amount of Sn incorporation, promoting the interaction of Pt and Sn.

The effect of Sn amount in the structure of catalysts for materials prepared by a deposition process using formic acid as the reducing agent could be inferred from the comparison of the lattice parameters of Pt_x–Sn_y/C and Pt/C (Table 1). For Pt_1–Sn_1/C catalyst, the lattice parameter changed, thus reflecting a Pt lattice expansion and the formation of a Pt-Sn alloy in some extent ($Pt_{1-x}Sn_x$ alloy; $x = 0.2$), thus indicating the lattice dilation of Sn atoms incorporated to the *fcc* lattice of Pt crystallites [38]. However, for Pt_3–Sn_1/C and Pt_2–Sn_1/C catalysts, the positions of the Pt peaks were almost equal to the Pt/C position, and the crystal line lattice parameters change little, indicating the absence of alloy formation between Pt and Sn. The lattice parameter displayed for Pt/C and Pt_1–Sn_1/C catalysts (0.3911 and 0.3980 nm, respectively) are in a good agreement with those of Pt and Pt_1Sn_1 nanosized particles [11, 19, 39]. It worth noting that the results obtained disagree with those in others studies, for instance, Comalti et al. [15, 36], where using a similar method for preparation of catalysts, Pt–Sn alloys were obtained for all amounts of Sn. This difference could be related to a small difference in preparation conditions.

3.1.2 TEM characterization

TEM micrographs and histograms of the catalysts are shown in Figures 2a–d, where the dark spots represent the Pt and Sn metals. The average sizes of the particles obtained by TEM (inset in Figure 2 and data in Table 1) agreed with values calculated from XRD patterns. Both XRD and TEM results indicate that all catalysts synthesized in this work are highly and uniformly dispersed on the carbon support, as well as with a narrow particle size range, thus demonstrating that the deposition method with formic acid as a reducing agent could provide an easy, inexpensive, and suitable way to prepare nanosized catalysts. All the Pt_x–Sn_y/C catalysts presented similar average particle sizes irrespective of Sn content. No significant change in the metal particle size with variations in the Sn amount during preparation was found, thus allowing the particle size effect to be excluded from the influential parameters for the electrocatalytic activity towards ethanol oxidation over Pt_x–Sn_y/C catalysts.

3.1.3 SEM and EDS characterization

The composition of the Pt_x–Sn_y/C catalysts was determined by EDS analysis. The EDS composition for each sample was obtained from an average of measurements from various parts of the nanoparticle powder (Table 1). All the EDS compositions of prepared catalysts are very close to the nominal values. Figure 3a–d shows the surface morphology of Pt_x–Sn_y/C catalysts acquired by means of scanning electron micrograph images. It is clear that the powders contain many irregular particles with an almost homogeneous size distribution. The morphological characters displayed for the Pt_1–Sn_1/C catalyst is different from other catalysts, which could be related to the Pt–Sn being partially alloyed since the morphology of this catalyst shows a block of particles close together.

3.1.4 XPS characterization

Figures 4, 5, and 6 show the XPS spectra of Pt 4f, Sn 3d, and O1s for Pt_x–Sn_y/C and Pt/C catalysts. XPS analysis provided information about catalyst surface composition. The XPS survey analysis of the catalysts, supporting information (SI), indicated that precursors are not on the catalyst surface after the preparation procedure (survey of Pt_3–Sn_1 is included in Figure SI as an example).

The Pt 4f spectral profiles are included in Figure 4, where the Pt 4f region displayed spin-orbital splitting of the $4f_{7/2}$ and $4f_{5/2}$ states. In Figure 4, the maximum energies of the main bands for all samples appear at 71.6 eV and 74.8 eV, suggesting the presence of metallic Pt. The binding energy values for metallic Pt are in agreement with published data [40]. The two broad profiles were deconvoluted into four different peaks with maxima at 71.5, 72.9, 74.8, and 76.0 eV, which correspond to different oxidation states of Pt. The deconvoluted peaks centered at 72.9 and 76.0 eV could be attributed to formation of Pt–O_{ad} bonds in Pt^{2+} (PtO or $Pt(OH)_2$) and Pt^{4+} (PtO_2) species, respectively [41], while the deconvoluted peaks at 71.5 and 74.7 eV were attributed to metallic Pt.

The binding energy of the metallic Pt peaks (71.5 eV) was slightly higher than typical values reported in the literature (70.7–71.1 eV) [42], which could be explained by the small particle size of Pt or by the interaction with Sn [43, 44]. This shift in binding energy with regard to pure Pt has also been attributed to Pt-support interactions, such as those seen for carbon or zeolite-supported Pt [45, 46]. The binding energies of metallic Pt for Pt_1–Sn_1 and Pt_2–Sn_1 (71.3 and 74.5 eV) were slightly lower than those of Pt/C (71.5 and 74.8 eV), while for Pt_3–Sn_1 (71.5 and 74.8 eV), the binding energies were equal. These XPS data indicate that the electronic structure of Pt was modified by Sn addition, and that it could be dependent on the amount of Sn content in the Pt_x–Sn_y/C catalysts. Kim et al. [19] reported charge transfer from the less-electronegative Sn to the more-electronegative Pt.

Figure 5 shows the Sn $3d_{5/2}$ signal deconvoluted into two different peaks. The Pt_1–Sn_1 and Pt_3-Sn_1 have a low BE peak centered at 485.6 eV, which was attributed to metallic Sn, and a primary high BE peak at 487.1 eV assigned to Sn^{4+} species [42], while for Pt_2–Sn_1, only the peak at 487.1 eV is observed. The higher percentage of Sn^{4+} species on Pt_x–Sn_y/C catalysts could be due to the strong affinity of tin towards oxygen species (oxophilicity), thereby being easily oxidized by dioxygen and/or H_2O from the atmosphere.

Figure 6 shows the XPS spectra of the O1s transition. For Pt_x–Sn_y/C catalysts, the O1s spectrum is resolved into three peaks centered at 530.0, 531.9, and 533.7 eV, while for the Pt/C catalyst, there are two peaks centered at 531.2 and 532.8 eV. It can be established that for Pt_x–Sn_y/C catalysts, the O1s represents three oxygen species in terms of the 1s signal, with the lower BE peak (530.0 eV) being assigned to lattice oxygen species (SnO_2 – Pt–O_{ad}), middle (531–532 eV) to adsorbed oxygen species (O^{2-}/O^{-}), and the higher peak (533–534 eV) to hydroxyl groups (OH^{-}) [47]. The O1s for Pt_x–Sn_y/C catalysts shifts from Pt/C due to the contribution of Sn for surface hydroxylation and therefore, the relative atomic structure composition of the various oxygen species is dependent on the presence of Sn on the catalyst surface.

The fraction of Pt and Sn species calculated from the relative intensities of deconvoluted and Pt/Sn surface composition observed from the XPS results are summarized in Table 2. Pt^0 is the predominant species (80–85%) in Pt_x–Sn_y/C and Pt/C catalysts, with small amounts of the oxidized Pt species (15–20%) that could be produced on the catalyst surface through a passivation process during the sample preparation. The surface atomic ratios obtained from XPS were close to those of the bulk compositions obtained by EDS. However, the surface Pt/Sn atomic ratios tended to be lower than the bulk values, indicating a clear enrichment of Sn in the outermost layers by segregation of Sn onto the surface, especially in the samples with higher Sn content. This behavior may be explained by thermodynamic concepts, since the nature of the Sn element has a lower surface free energy than platinum, thus producing migration of Sn from the bulk to the surface [19]. Another reason could be explained in terms of the different kinetics of the reduction process of the platinum and tin. If the deposition method is adopted for Pt and Sn reduction, the $PtCl_6^{\ 2-}$ ion is easier than Sn^{4+}, and then some of the Pt active sites may be blocked by Sn atoms. Finally, it possible to establish that the structures of Pt_x–Sn_y particles on the surface catalyst consist of a Sn-rich surface layer and a Pt-rich inner part.

3.1.5 CO stripping

Figure 7 shows CO stripping voltammograms of catalysts recorded at 10 mV s^{-1} in the supporting electrolyte at room temperature. Currents are expressed in terms of geometric surface area. There are two anodic waves for CO stripping for the Pt/C catalyst, with the onset of CO oxidation close to 0.40 V (*vs.* RHE), and a broad stripping current peak is seen at 0.61 V (*vs.* RHE) with a maximum of the oxidation peak at 0.48 and 0.77 V (*vs.* RHE), respectively. For Pt_x–Sn_y/C catalysts, the onset of CO oxidation occurs at a lower potential, close to 0.27 V (*vs.* RHE) and maximum peaks are dependent on the Sn amount. The lower potential on the Pt_x–Sn_y/C catalysts is attributed to the presence of oxygenated species on Sn sites that are formed at lower potentials compared to platinum [48, 49], which allows the oxidation of CO to CO_2 at lower potentials according to the bifunctional mechanism [50]. The oxidation of adsorbed CO occurs over a relatively large potential range on Pt_x–Sn_y/C in comparison to Pt/C, where the adsorbed CO monolayer is oxidized in narrow current peaks. According to Massong et al. [51], this effect is due to the presence of adsorbed CO_L (linearly bonded CO) and CO_B (bridge-bonded CO) on Pt sites. They claim that on Pt–Sn, CO_B can be oxidized at lower potentials than on Pt. The shape of the CO stripping peak depends strongly on the nature of the catalyst. Different peaks and/or shoulders presented by CO stripping voltammograms could also be related to heterogeneous sites on the catalyst surface.

The onset potential of CO oxidation is about the same for Pt_x–Sn_y/C catalysts, independently of the Sn content in the material. This result is in agreement with the report of Crabb et al. [52] who found that the onset potential of carbon monoxide oxidation is lowered with the addition of a small amount of tin to platinum, and small changes in terms of shift potential are observed as quantities of tin are increased. The lower potential observed for CO oxidation with the Pt_x–Sn_y/C catalysts are in agreement with data reported by Colmati et al. [15], although the shape of the profiles is different despite the methodology used for preparation materials being similar. Finally, according to the profiles of CO stripping, there is no clear evidence that the Pt–Sn alloy and/or Pt and non-alloyed SnO_2 phase contribute any significant activity for CO oxidation in these catalysts.

The electrochemical active surface (EAS) areas were estimated with assumptions that the normalized charge density for a monolayer of adsorbed carbon monoxide on polycrystalline platinum is 420 $\mu C*cm^{-2}$ and all platinum loaded on the working electrode is considered electrochemically active. Table 2 summarizes the EAS values with the Sn content, which was obtained using the CO desorption areas in the Pt–CO oxidation region. An increase of EAS with the addition of Sn in the composition of the catalyst can be observed for Pt_x–Sn_y/C catalysts, so a higher amount of Pt is indeed available. The highest EAS values were displayed for Pt_2–Sn_1 and Pt_3–Sn_1 catalysts, while for the Pt_1–Sn_1 catalyst, the EAS value was increased twofold with respect to Pt/C. This behavior is in contrast to that shown in [19, 36], where the EAS dropped for the highest Sn-containing Pt_1–Sn_1 catalyst.

3.2 Electrochemical characterization

Figure 8 shows cyclic voltammograms obtained in 0.5 M H_2SO_4 at a scan rate of 0.02 V s^{-1} for all catalysts. Since different amounts of metal loading are loaded onto the working electrode for all tests, the currents were normalized by the geometric area of the working electrode (*i.e.*, current density) and the total amount of Pt. The voltammograms display the typical behavior of the hydrogen and oxide regions of Pt in these kinds of materials in acid solution [53]. The adsorption/desorption of hydrogen between 0.05 and 0.40 V (*vs*. RHE) was seen for all catalysts. For Pt_x–Sn_y/C catalysts, a large value for the double-layer charging current (0.4–0.8 V) was observed, indicating that all the catalysts have a similar double-layer capacitance, which can be attributed to the presence of tin oxides on the particle surface that increases electrode capacitance [53]. The region of hydrogen-desorption for Pt_1–Sn_1/C was not well defined, as expected from the high degree of alloying of the Sn-containing catalysts [36]. For other catalysts, the shape of peaks in the electrochemical profiles appears to be independent of Pt amount, which could indicate the same Pt species on the surface of the catalysts.

It is well established that the rate-determining steps in the electro-oxidation of ethanol at low temperature in the acid environment [54] for platinum catalyst is limited by the ability for C–C bond cleavage and CO oxidation. Electronic and/or structural modifications of Pt with a second metal, such as Sn, would be largely effective towards electro-oxidation as shown in Figure 9 for cyclic voltammograms of Pt_x–Sn_y/C catalysts. The shapes of the curves are typical for the ethanol electro-oxidation reaction, showing two anodic current peaks in positive and negative sweeps, respectively, which are related to the oxidation reaction of ethanol in the positive sweep and the incomplete oxidized carbonaceous residues on the catalyst surface during the negative sweep. The latter intermediates are likely to be strongly adsorbed on the Pt surface, covering active surface sites of Pt for the next round, thus making the anodic reactions more sluggish. The addition of Sn into Pt leads to substantial enhancements in the catalytic activity towards the ethanol electro-oxidation, in agreement with results presented by different authors [10–13].

Chronoamperometry measurements were performed at 0.6 V (*vs*. RHE) to compare the catalytic activity of the anode catalysts (Figure 10). During the first seconds, there was a sharp decrease in the current density, followed by a slow decrease in the current density and a steady-state current was observed for all catalysts after ~300 s. This can be explained by the fact that at first, the dehydrogenation process of ethanol occurs irreversibly at the Pt sites leading to some strongly adsorbed intermediates. This reaction competes with the activation of interfacial water preferentially at the Sn sites, which is necessary for the removal of these irreversibly adsorbed species (CO, for example) from the electrode surface [18, 33]. The chronoamperometric curve for Pt/C displays a faster decrease than that for the other catalysts. The Pt_2–Sn_1/C catalyst presented higher activity, whereas similar behaviors for the Pt_3–Sn_1/C and Pt_1–Sn_1/C catalysts were seen. Figure 11 shows anodic polarization curves. The onset potential of ethanol electro-oxidation using Pt_x–Sn_y/C was shifted negatively by ~0.2 V in comparison to Pt/C. The behavior is similar for all catalysts and no effect of the amount of Sn in the electroactivity was found.

The results obtained through electrochemical measurements show that Sn contents in the catalysts have a different effect on the physical-chemical properties and in the ethanol electro-oxidation. For the Pt_1–Sn_1/C catalyst, XRD and SEM (Figure 1 and 3) indicate that the geometric environment was changed with Sn addition to the fcc-Pt crystallites by forming a solid solution of the Pt-Sn alloy phase, accompanying an expansion of lattice parameters (structural modification). This elongation of the bonding structure may affect the catalytic reaction pathways that require specific geometric arrangements of the surface atoms, thus leading to a change in the catalytic properties, which can catalyze the cleavage of C–C bond and/or CO oxidation (or CO-like intermediates) by increasing the amount of surface oxygen-containing species [19]. For lower and intermediate contents of Sn, Pt_3–Sn_1/C and Pt_2–Sn_1/C, from XPS results, show a decrease in Pt 4f binding energy (Figure 4) of Pt_x–Sn_y/C catalysts, especially for Pt_2–Sn_1 and Pt_3–Sn_1 with respect to the Pt/C catalyst, which can be attributed to charge transfer from Sn to Pt [19]. This weaker bond between Pt and Sn atoms (electronic structure modification) can cause a prevention or reduction of catalytic poisoning by electronic effects (filling part of the Pt *d*-band vacancies), which are the main advantages of these bimetallic Pt–Sn catalysts. Moreover, the tin content at the vicinity of the Pt sites in the bimetallic composition contributes to a bifunctional reaction process that favors an oxygenated-donor effect on the removal of the adsorbed species at the Pt surface and the contribution to the formation of acetic acid [55].

The deposition process using formic acid as the reducing agent used in this work for synthesis of Pt_x–Sn_y/C and Pt/C catalysts showed that both, the amount of tin present in the catalyst composition modifies in different grade the structure of catalysts and does not show variation in the electroactivity towards ethanol oxidation. Similar methodologies applied for synthesis of Pt_x–Sn_y/C catalysts with a small change (for example, time and/or concentration of reduction agent) show differences with the results obtained, thus highlighting the importance of the conditions of the preparation method. For instance, the results presented by Zignani et al. [17] and Colmati et al. [15, 36] showed that for the Pt_x–Sn_y/C catalysts, a larger particle size and a higher degree of alloying is observed when increasing the amount of Sn. Moreover, the activity for the ethanol oxidation reaction depended on the amount of both non-alloyed and alloyed Sn.

4. Conclusions

The deposition process using formic acid as the reducing agent used for synthesis of Pt_x–Sn_y/C and Pt/C catalysts highlights the importance of conditions on preparation method. For the Pt_1–Sn_1/C catalyst, there was a change in the lattice parameter, which reflects the lattice expansion, while for Pt_3–Sn_1/C and Pt_2–Sn_1/C catalysts the electronic structure of Pt was modified by Sn addition. The promoting effects and mechanism of Sn incorporation depend on catalyst preparation and the Sn/Pt ratio. The presence of metals as Pt–M alloys or Pt–M bimetallic catalysts improves the catalytic effect of platinum due to the bifunctional mechanism. The Pt_x–Sn_y/C catalyst with an atomic ratio of 1:1 was best, and contributed to reducing the amount of noble metal in the anode of direct alcohol fuel cells. All catalysts synthesized are highly and uniformly dispersed and in a narrow particle size range on the carbon support, demonstrating that the deposition method with formic acid as reducing agent could provide an easy, inexpensive, and suitable way to prepare nanosized catalysts.

Acknowledgements

The authors thank the Brazilian National Council of Technological and Scientific Development-CNPq (grants: 303630/2012-4, 402243/2012-9 and 310282/2013-6) for the scholarships and financial support for this work and Universidad de Antioquia by its financial support through the "Sostenibilidad 2014-2015" program.

References

[1] K.B. Prater, J. Power Sources 61 (1996) 105-109.

[2] F. Simões, D. Dos Anjos, F. Vigier, J.M. Léger, F. Hahn, C. Coutanceau, E. Gonzalez, G. Tremiliosi-Filho, A. De Andrade, P. Olivi, J. Power Sources 167 (2007) 1-10.

[3] C. Lamy, Electrochim. Acta 29 (1984) 1581-1588.

[4] E. Antolini, E. Gonzalez, Catal. Today 160 (2011) 28-38.

[5] F. Vigier, C. Coutanceau, A. Perrard, E. Belgsir, C. Lamy, J. Appl. Electrochem. 34 (2004) 439-446.

[6] A.O. Neto, M. Giz, J. Perez, E. Ticianelli, E. Gonzalez, J. Electrochem. Soc. 149 (2002) A272-A279.

[7] M. González Pereira, M. Dávila Jiménez, M. Elizalde, A. Manzo-Robledo, N. Alonso-Vante, Electrochim. Acta 49 (2004) 3917-3925.

[8] G. Camara, R. De Lima, T. Iwasita, Electrochem. Commun. 6 (2004) 812-815.

[9] W. Zhou, S. Song, W. Li, G. Sun, Q. Xin, S. Kontou, K. Poulianitis, P. Tsiakaras, Solid State Ionics 175 (2004) 797-803.

[10] F. Delime, J. Leger, C. Lamy, J. Appl. Electrochem. 29 (1999) 1249-1254.

[11] W. Zhou, Z. Zhou, S. Song, W. Li, G. Sun, P. Tsiakaras, Q. Xin, Appl. Catal. B. Environ. 46 (2003) 273-285.

[12] W. Zhou, S.Q. Song, W.Z. Li, Z.H. Zhou, G. Sun, Q. Xin, S. Douvartzides, P. Tsiakaras, J. Power Sources 140 (2005) 50-58.

[13] L. Jiang, G. Sun, S. Sun, J. Liu, S. Tang, H. Li, B. Zhou, Q. Xin, Electrochim. Acta 50 (2005) 5384-5389.

[14] F.E. López-Suárez, A. Bueno-López, K.I.B. Eguiluz, G.R. Salazar-Banda, J. Power Sources 268 (2014) 225-232.

[15] F. Colmati, E. Antolini, E.R. Gonalez, J. Electrochem. Soc. 154 (2007) B39-B47.

[16] F. Colmati, E. Antolini, E.R. Gonzalez, Appl. Catal. B. Environ. 73 (2007) 106-115.

[17] S. Zignani, E. Gonzalez, V. Baglio, S. Siracusano, A. Aricò, Int. J. Electrochem. Sci. 7 (2012) 3155-3166.

[18] J. Ribeiro, D. Dos Anjos, K.B. Kokoh, C. Coutanceau, J.-M. Léger, P. Olivi, A. De Andrade, G. Tremiliosi-Filho, Electrochim. Acta 52 (2007) 6997-7006.

[19] J.H. Kim, S.M. Choi, S.H. Nam, M.H. Seo, S.H. Choi, W.B. Kim, Appl. Catal. B. Environ. 82 (2008) 89-102.

[20] F. Vigier, C. Coutanceau, F. Hahn, E. Belgsir, C. Lamy, J. Electroanal. Chem. 563 (2004) 81-89.

[21] C. Lamy, S. Rousseau, E. Belgsir, C. Coutanceau, J.-M. Léger, Electrochim. Acta 49 (2004) 3901-3908.

[22] L. Jiang, G. Sun, Z. Zhou, W. Zhou, Q. Xin, Catal. Today 93 (2004) 665-670.

[23] H. Liu, C. Song, L. Zhang, J. Zhang, H. Wang, D.P. Wilkinson, J. Power Sources 155 (2006) 95-110.

[24] C. Lamy, A. Lima, V. LeRhun, F. Delime, C. Coutanceau, J.-M. Léger, J. Power Sources 105 (2002) 283-296.

[25] A. Verma, S. Basu, J. Power Sources 145 (2005) 282-285.

[26] E.V. Spinacé, L.A. do Vale, R.R. Dias, A.O. Neto, M. Linardi, Stud. Surf. Sci. Catal. 162 (2006) 617-624.

[27] Y. Wang, S. Song, G. Andreadis, H. Liu, P. Tsiakaras, J. Power Sources 196 (2011) 4980-4986.

[28] J.-M. Léger, S. Rousseau, C. Coutanceau, F. Hahn, C. Lamy, Electrochim. Acta 50 (2005) 5118-5125.

[29] H. Bönnemann, G. Braun, W. Brijoux, R. Brinkmann, A.S. Tilling, K. Seevogel, K. Siepen, J. Organomet. Chem. 520 (1996) 143-162.

[30] I. Capek, Adv. Colloid Interface Sci. 110 (2004) 49-74.

[31] K. Okitsu, A. Yue, S. Tanabe, H. Matsumoto, Chem. Mat. 12 (2000) 3006-3011.

[32] Z. Liu, X.Y. Ling, J.Y. Lee, X. Su, L.M. Gan, J. Mat. Chem. 13 (2003) 3049-3052.

[33] Z. Liu, B. Guo, L. Hong, T.H. Lim, Electrochem. Commun. 8 (2006) 83-90.

[34] H. Bönnemann, W. Brijoux, R. Brinkmann, T. Joußen, B. Korall, E. Dinjus, Angew. Chem. Int. Ed. (English) 30 (1991) 1312-1314.

[35] F. Purgato, P. Olivi, J.-M. Léger, A. De Andrade, G. Tremiliosi-Filho, E. Gonzalez, C. Lamy, K. Kokoh, J. Electroanal. Chem. 628 (2009) 81-89.

[36] F. Colmati, E. Antolini, E.R. Gonzalez, Electrochim. Acta 50 (2005) 5496-5503.

[37] G.R. Salazar-Banda, K.I. Eguiluz, M. Pupo, H.B. Suffredini, M.L. Calegaro, L.A. Avaca, J. Electroanal. Chem. 668 (2012) 13-25.

[38] I.G. Casella, E. Desimoni, Electroanal. 8 (1996) 447-453.

[39] V. Radmilovic, T. Richardson, S. Chen, P. Ross Jr, J. Catal. 232 (2005) 199-209.

[40] S. Hüfner, G. Wertheim, Phys. Rev. B. 11 (1975) 678.

[41] S. Sun, D. Yang, D. Villers, G. Zhang, E. Sacher, J.P. Dodelet, Adv. Mat. 20 (2008) 571-574.

[42] http://www.lasurface.com, (July, 2014).

[43] M. Goetz, H. Wendt, J. Appl. Electrochem. 31 (2001) 811-817.

[44] C. Roth, M. Goetz, H. Fuess, J. Appl. Electrochem. 31 (2001) 793-798.

[45] E. Antolini, L. Giorgi, F. Cardellini, E. Passalacqua, J. Solid State Electrochem. 5 (2001) 131-140.

[46] J.C. Vedrine, M. Dufaux, C. Naccache, B. Imelik, J. Chem. Soc., Faraday Trans. 1 74 (1978) 440-449.

[47] T.L. Barr, The J. Phys. Chem. 82 (1978) 1801-1810.

[48] Y. Morimoto, E.B. Yeager, J. Electroanal. Chem. 441 (1998) 77-81.

[49] K. Wang, H. Gasteiger, N. Markovic, P. Ross, Electrochim. Acta 41 (1996) 2587-2593.

[50] H.A. Gasteiger, N. Markovic, P.N. Ross Jr, E.J. Cairns, J. Phys. Chem. 98 (1994) 617-625.

[51] H. Massong, H. Wang, G. Samjeské, H. Baltruschat, Electrochim. Acta 46 (2001) 701-707.

[52] E. Crabb, M. Ravikumar, D. Thompsett, M. Hurford, A. Rose, A. Russell, Phys. Chem. Chem. l Phys. 6 (2004) 1792-1798.

[53] D. Stevens, J. Dahn, J. Electrochem. Soc. 150 (2003) A770-A775.

[54] J. Kua, W.A. Goddard, J Amer. Chem. Soc. 121 (1999) 10928-10941.

[55] F. Purgato, S. Pronier, P. Olivi, A. De Andrade, J. Léger, G. Tremiliosi-Filho, K. Kokoh, J. Power Sources 198 (2012) 95-99.

Figure captions

Figure 1. X-ray diffractograms of samples over the scan range 10-90º.

Figure 2. TEM images and histogram of particle size distribution determined from TEM of Pt/C (a), $Pt_1–Sn_1$ (b), $Pt_2–Sn_1$ (c), and $Pt_3–Sn_1$ (d) catalysts.

Figure 3. SEM images of Pt/C (a), $Pt_1–Sn_1$ (b), $Pt_2–Sn_1$ (c), and $Pt_3–Sn_1$ (d) catalysts.

Figure 4. Pt 4f transition in XPS experiments performed with catalysts.

Figure 5. Sn 3d transition in XPS experiments performed with catalysts.

Figure 6. O 1s transition in XPS experiments performed with catalysts.

Figure 7. CO stripping experiments recorded at 0.01 V $s^{–1}$.

Figure 8. Cyclic voltammetry curves for electrocatalysts in 0.5 M H_2SO_4 electrolyte. Scan rate of 0.02 V $s^{–1}$ at room temperature.

Figure 9. Cyclic voltammetry curves (anodic and forward sweep) recorded for ethanol oxidation in the 0.50 M C_2H_5OH/0.5 M H_2SO_4 solution. Scan rate of 0.02 V $s^{–1}$ at room temperature.

Figure 10. Chronoamperometric curves for the oxidation of ethanol in 0.5 M C_2H_5OH/0.5 M

H_2SO_4 solution at 0.6 V (b) *versus* RHE at room temperature.

Figure 11. Anode polarization profiles for the oxidation of ethanol in 0.50 M C_2H_5OH/0.5 M H_2SO_4 solution at room temperature.

Table

Table 1

Structural characteristic obtained from XRD, TEM and EDS.

Catalyst	EDS composition (%)	Particle size (nm)[a]	Lattice parameter (nm)	Average particle size from TEM (nm)
Pt/C	100	5.4	0.3911	3.89 ± 1.04
Pt_1Sn_1	66:34 (62:38) [b]	3.1	0.3980	3.95 ± 1.63
Pt_2Sn_1	78:22 (77:23) [b]	3.9	0.3918	3.19 ± 0.65
Pt_3Sn_1	82:18 (83:17) [b]	4.7	0.3919	3.36 ± 0.59

[a] Calculated from Pt (220) peak with the Scherrer's formula.

[b] Nominal percentage.

Table

Table 2

Percentage of different Pt and Sn species observed from the XPS data and EAS values.

Catalyst	Pt^0 / Pt^{2+} species (%)	Sn^0/ Sn^{4+} species (%)	Pt/Sn (atomic ratio)	EAS (m^2 gr_{Pt}^{-1})[a]
Pt/C	85 /15	-	-	13
Pt_1–Sn_1	80 / 20	10 / 90	0.62	25
Pt_2–Sn_1	85 / 15	100	1.52	31
Pt_3–Sn_1	83 / 17	15 / 85	2.78	32

[a] Calculated from CO stripping experiments assuming that the normalized charge density for a monolayer of adsorbed carbon monoxide on polycrystalline platinum is 420 $\mu C*cm^{-2}$

Figure

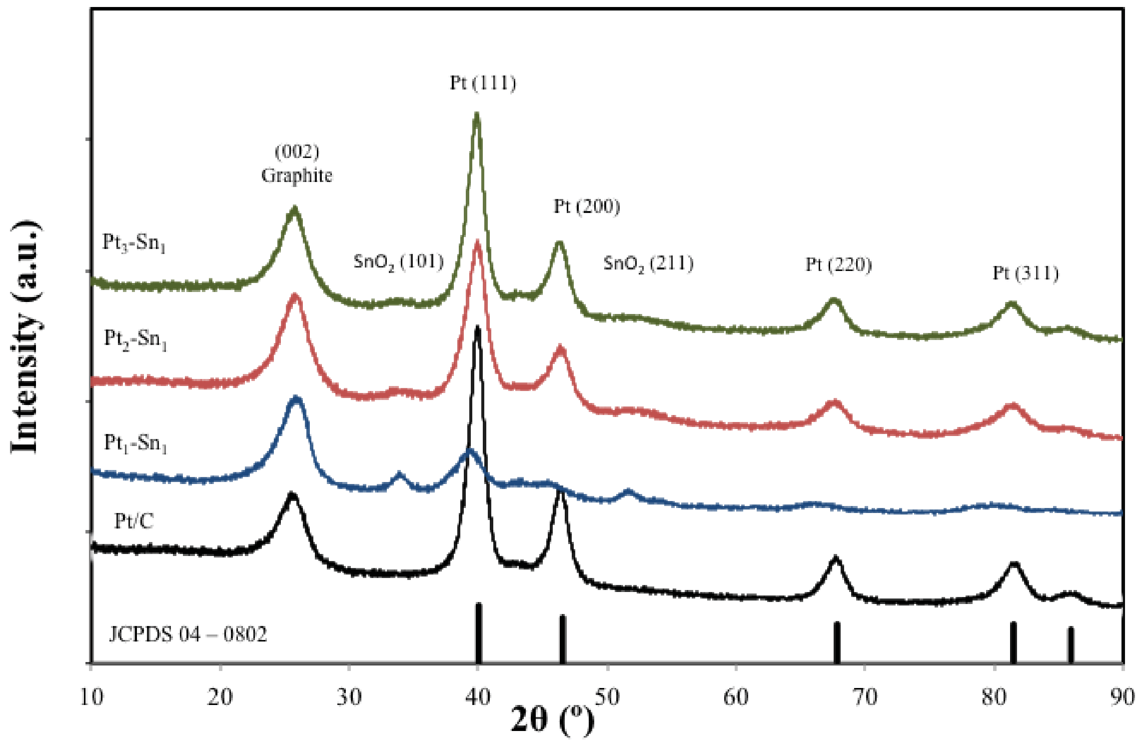

Figure 1.

Figure

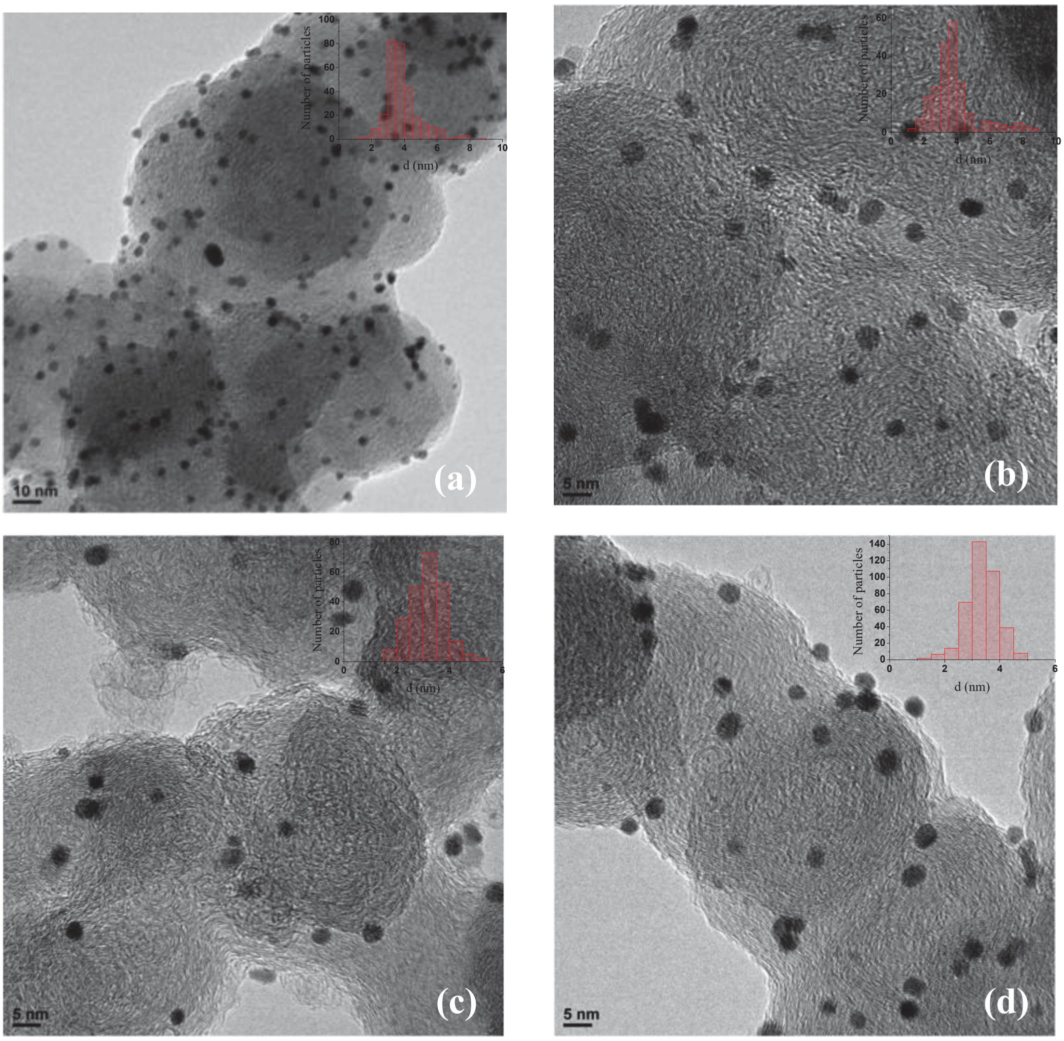

Figure 2.

Figure

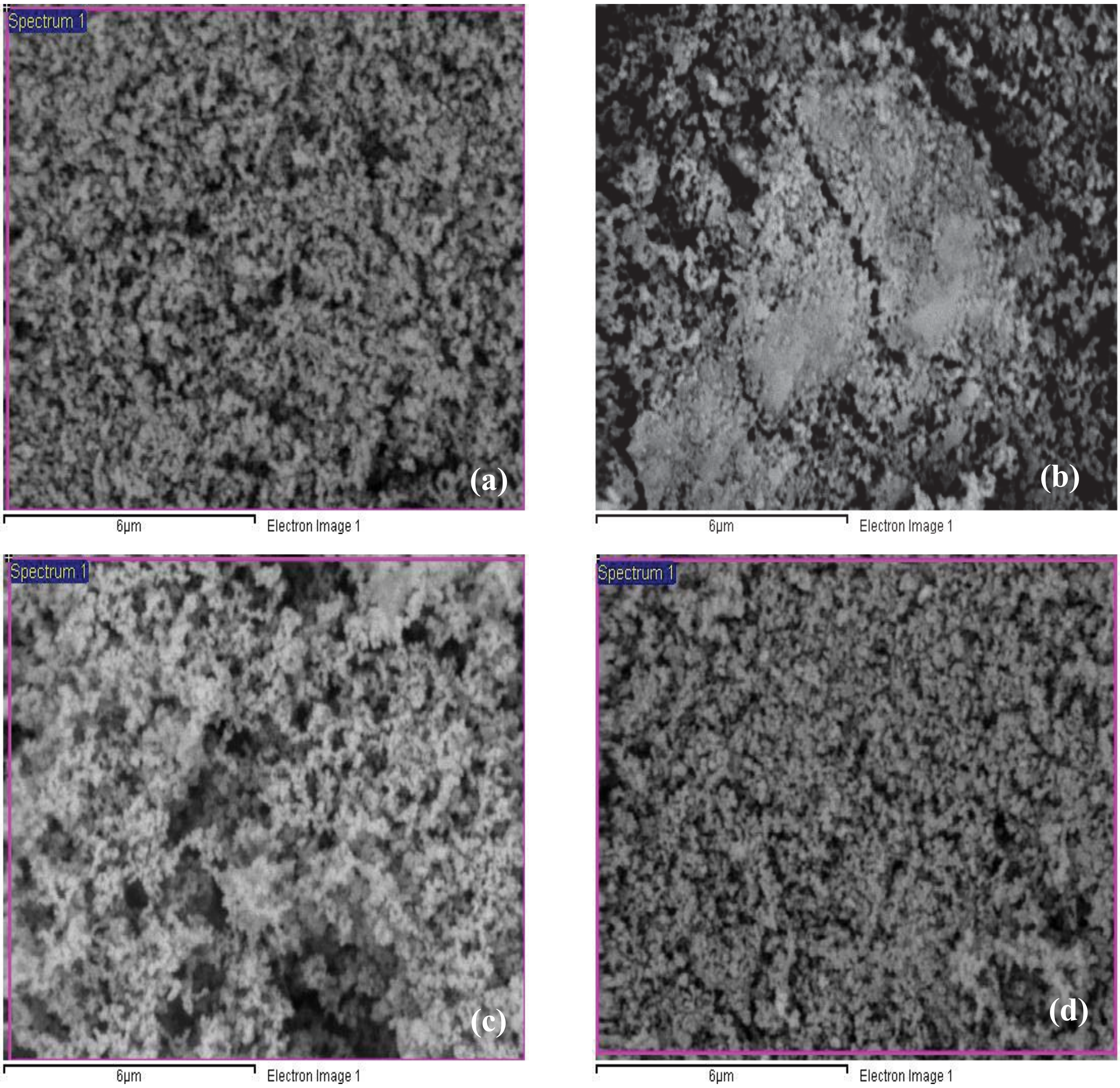

Figure 3.

Figure

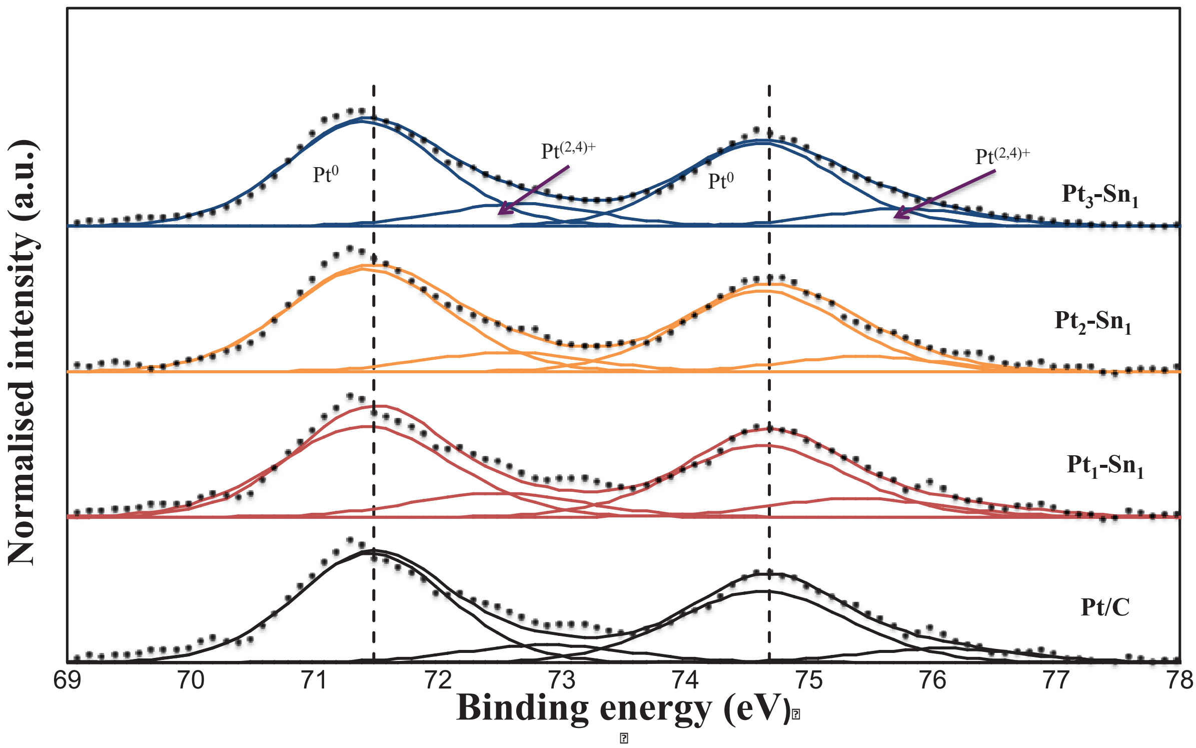

Figure 4.

Figure

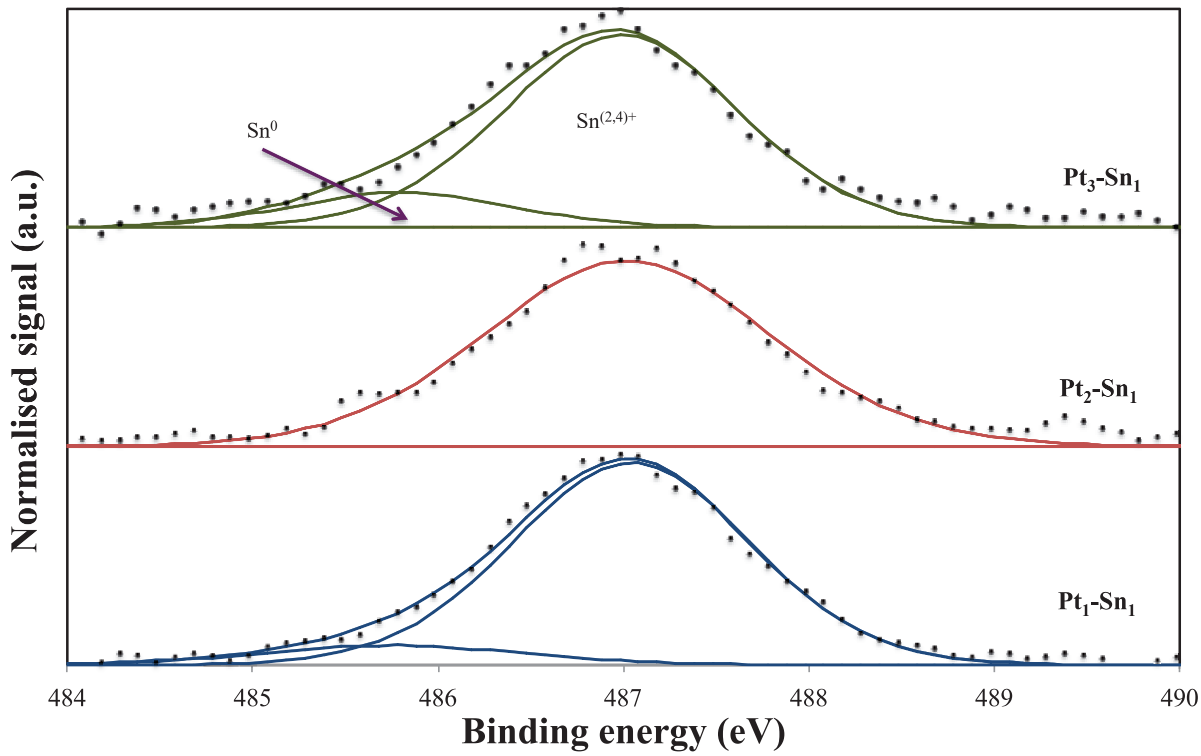

Figure 5.

Figure

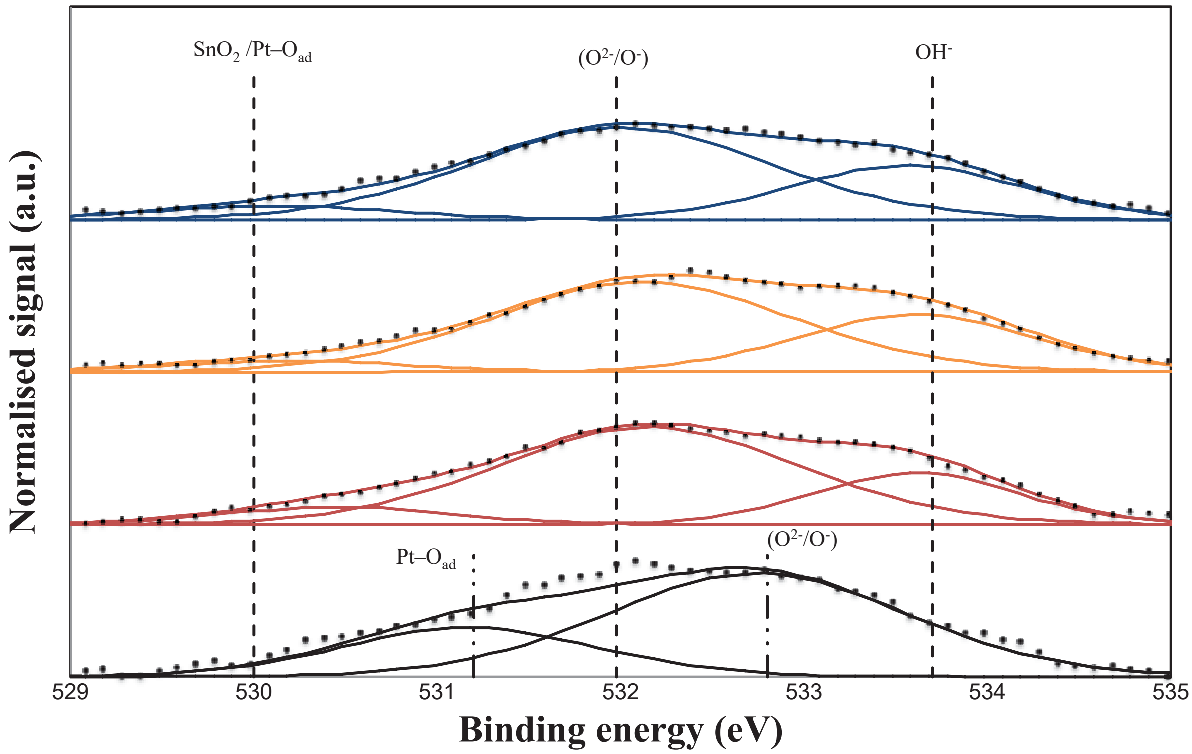

Figure 6.

Figure

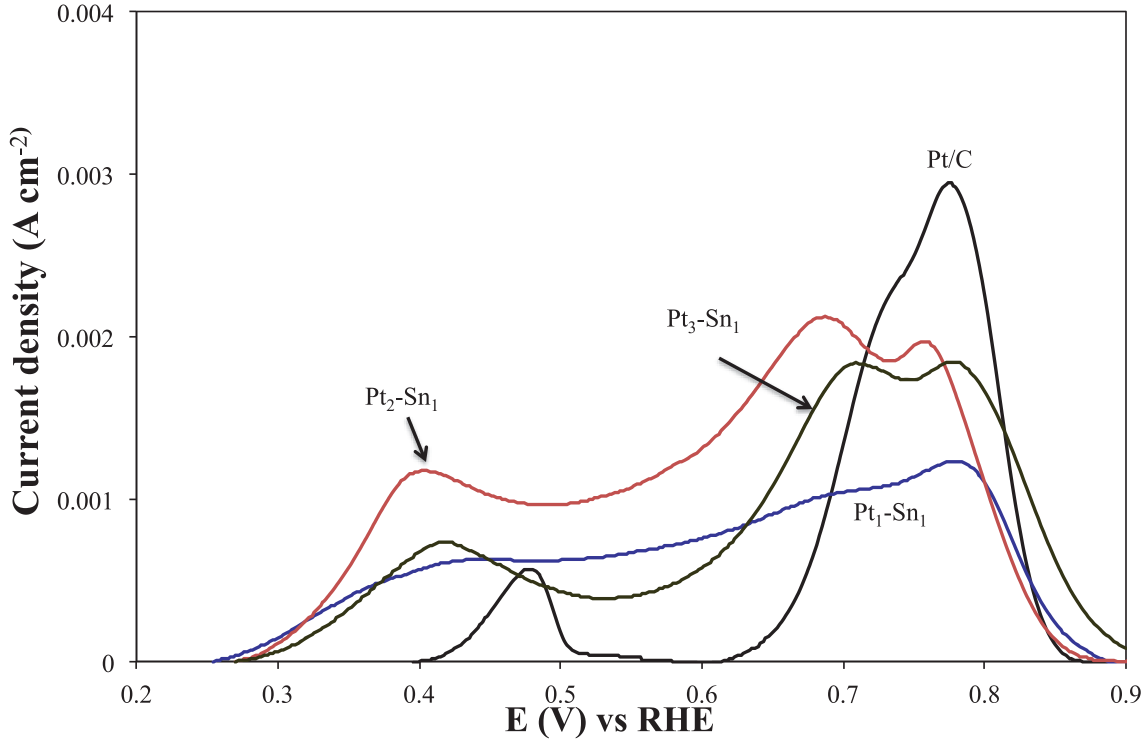

Figure 7.

Figure

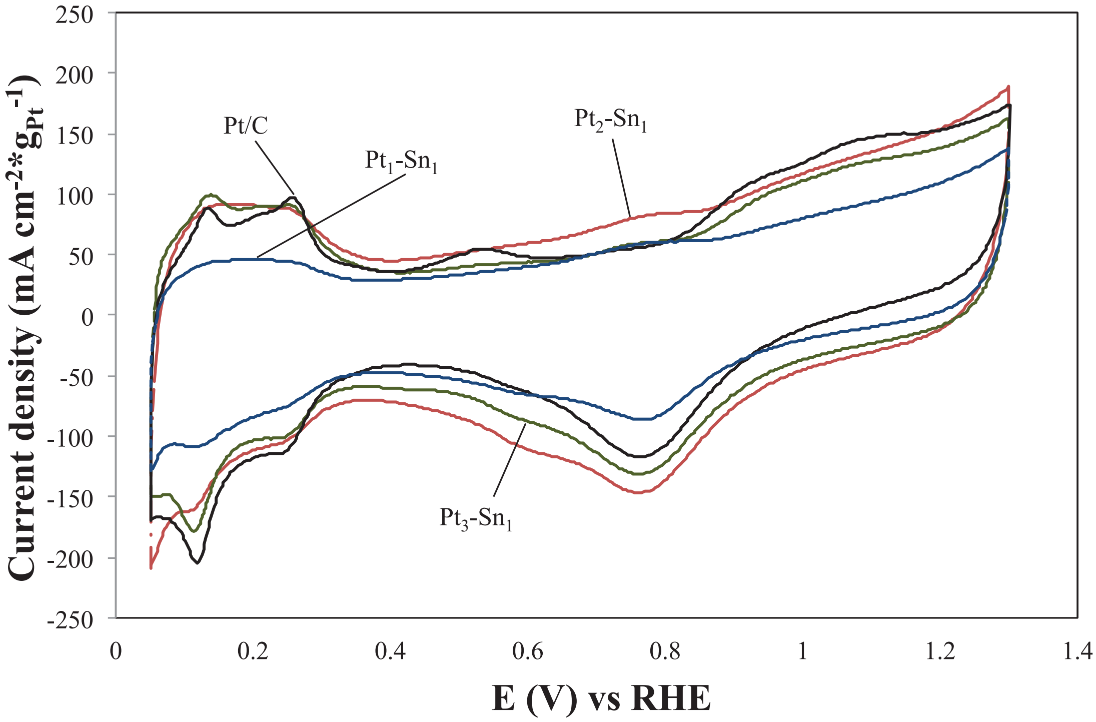

Figure 8.

Figure

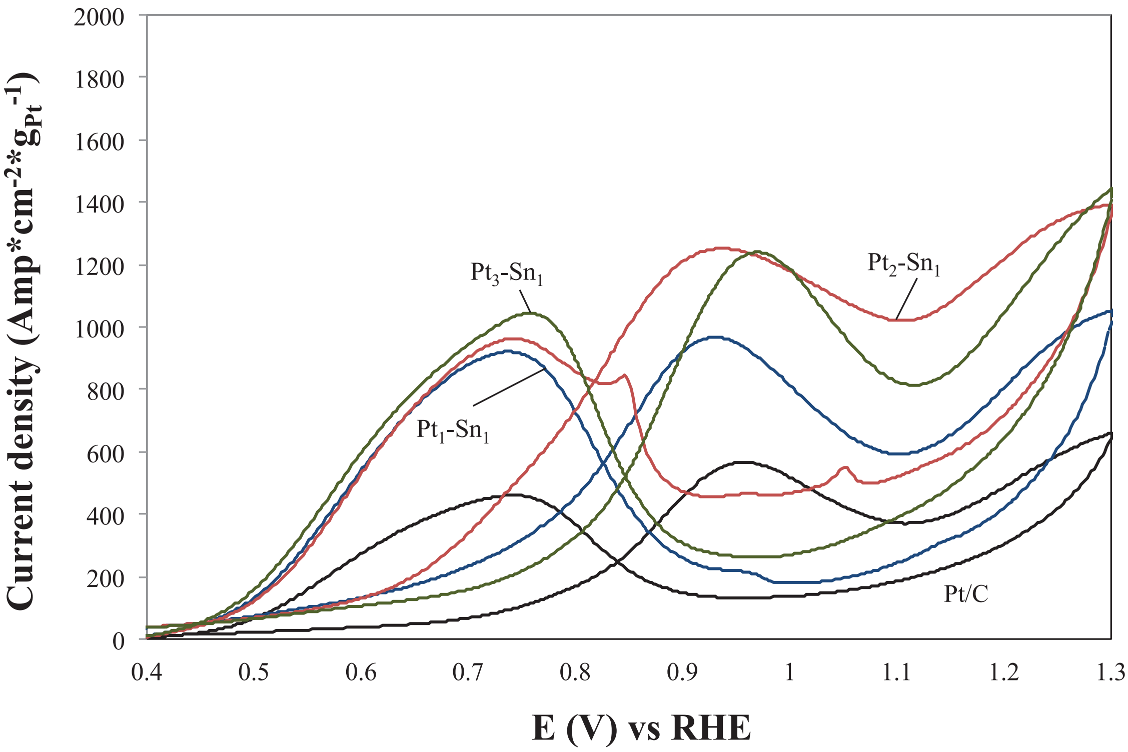

Figure 9.

Figure

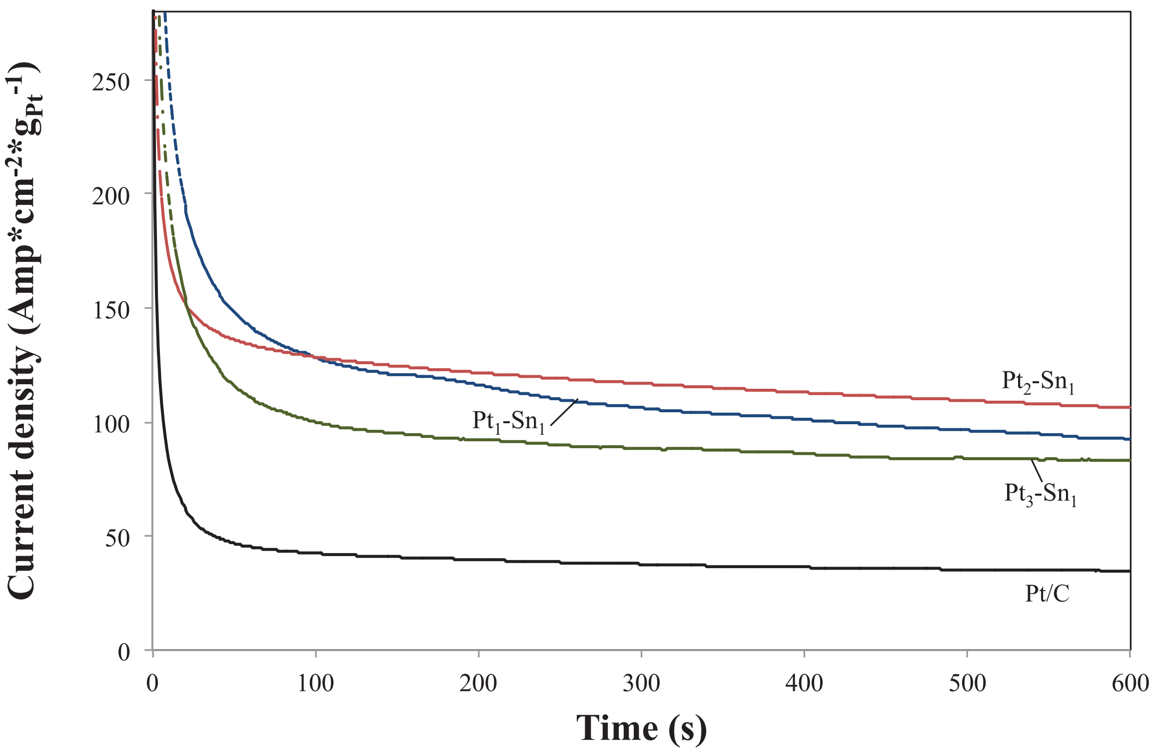

Figure 10.

Figure

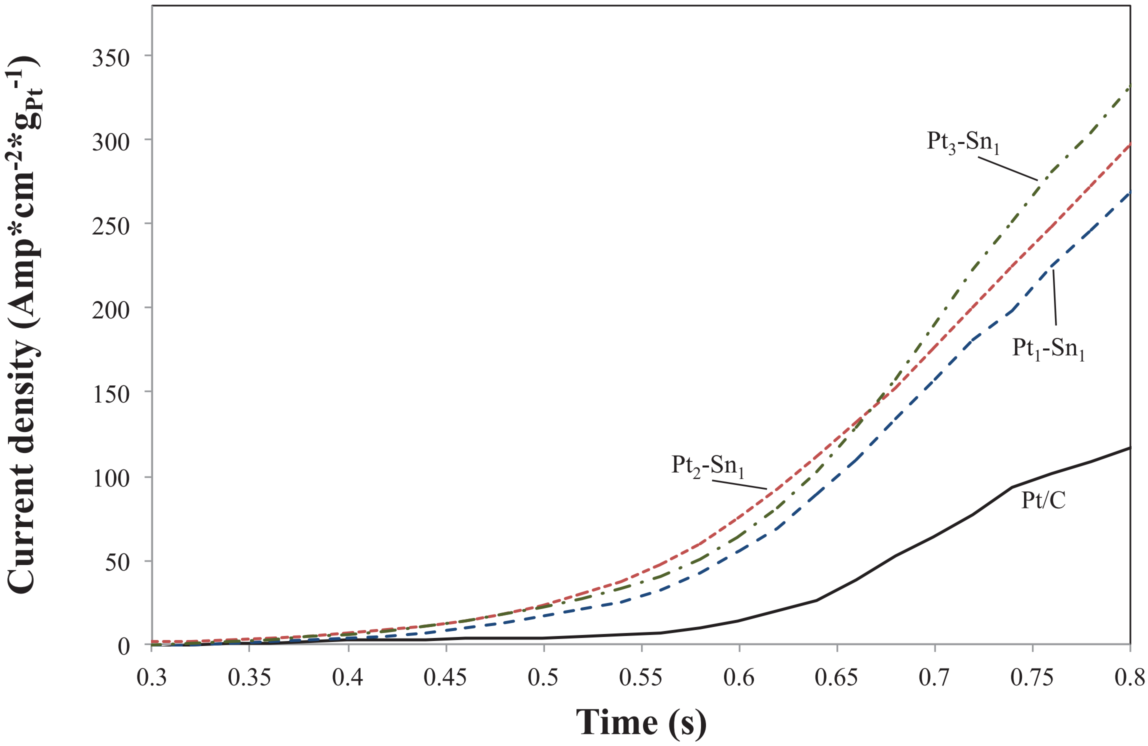

Figure 11.